2025 Caltech Report to SCEC

SCEC Award: 25108

High Resolution Catalogs of Template Earthquakes and Focal Mechanisms for Resolving Fine-Scale Fault Structures and Crustal Rheology

Principal Investigator

Egill Hauksson

California Institute of Technology, Seismological Laboratory, Pasadena, CA 91125

hauksson@caltech.edu

11 March 2026

Caltech Report for SCEC Award: 25108

Summary

We have refined and updated the catalogs of earthquake hypocenters (*Hauksson et al*., 2012) and focal mechanisms (*Yang et al.,* 2012) for southern California. The SCEC community will use the updated catalogs to address research problems, such as fine-scale fault structures, source studies, and crustal rheological properties, as well as applying template matching to generate high resolution catalogs.

The SCSN waveform relocated catalog that consists of 45 years of ~832,000 relocated earthquakes includes events in the SCSN reporting box. It includes aftershock sequences from four (M>7) mainshocks, 1992 Landers, 1999 Hector Mine, 2010 El Mayor-Cucapah, and 2019 Ridgecrest. This seismicity forms complex spatial and temporal patterns related to Pacific North America plate boundary tectonics processes. All of the M>7 mainshocks and regional seismicity that occurred across southern California, image the width of the plate boundary crustal deformation zone. In general, the smaller magnitude background seismicity occurs across southern California region of low stress, elevated strain rate and heat flow.

The 45-year catalog of first motions and S/P-ratio amplitudes focal mechanisms contains more than ~197,300 events of quality A, B, C, D. The focal mechanisms map regions of predominantly strike-slip faulting along the San Andreas Fault system. Limited regions of dip-slip or normal and reverse faulting are also identified, which are mostly related to geometrical complexities of the plate boundary. The stress field determined from the focal mechanism catalog is similar to the regional GNSS strain field but provides additional near fault spatial resolution of local stress field variations.

Previously these catalogs have been used for numerous studies such as: a) monitoring of temporal and spatial evolution of seismicity (*Hauksson et al.,* 2022), b) mapping of the geophysical properties of fault zones (*Plesch et al*., 2020), c) 3D velocity model inversions (*Tape et al.,* 2009), d) stress drop determinations, (*Shearer et al,* 2022), e) rheological properties of the crust, (*Hauksson and Meier*, 2018), f) earthquake statistics, *Zaliapin and Ben-Zion* (2020), g) identification and monitoring of anthropogenic seismicity.(*Chen et al,* 2011), h) aftershock studies (*van der Elst and Shaw*, 2015), and i) stress field determination (*Yang and Hauksson*, 2013).

This research continues to provide a more detailed understanding of earthquake source properties and their temporal variations. In addition, it will contribute to the CFM, SCEC 3D velocity model, stress model, rheology model, and understanding of fault zone processes. In the case of a major earthquake, improved absolute and relative locations will provide rapid identification of the rupture planes. In addition, events in this catalog will be used as templates in machine learning algorithms to search for previously undetected smaller events, which could on average add up to a factor of 10 more events to the catalog (*Ross et al*., 2019).

Results: Relocated earthquake (1981-2025)

The waveform relocated (1981 – 2025) Hauksson & Shearer (HS) catalog (*Hauksson et al.* 2012) of 741,000 GrowClust earthquakes is shown in Figure 1. It is produced via the following steps: (1) Initial locations are computed using existing phase picks and a 1d *P* and *S* velocity crustal model of *Hauksson* (2000) when applying the Hypoinverse program (*Klein*, 2002); (2) refined locations are computed using existing phase picks and a 3d *P* and *S* velocity crustal model applying the Simulps program (*Thurber,* 1993); (3) We divide the study region into 13 overlapping boxes for parallel processing. For all events in each box, waveform cross-correlation is performed for 750 nearest neighbors or all events on both *P* and *S* arrivals; Similar event clusters are identified based on the waveform correlation coefficients of 0.6 or greater; and (4) Events are separately relocated within each similar event cluster using the waveform cross-correlation times and an L1-norm method as applied in the GrowClust program (*Trugman and Shearer*, 2017). The final catalog is complete because it includes all events detected and located within the reporting region of the Southern California Seismic Network (SCSN). In the final catalog the three different types of solutions are labeled by their location box and location method: 1d, 3d, and gc. Only the gc solutions are in a GrowClust format while the others are in their native format. The relocated catalog can be downloaded from here:

http://scedc.caltech.edu/research-tools/alt-2011-dd-hauksson-yang-shearer.html

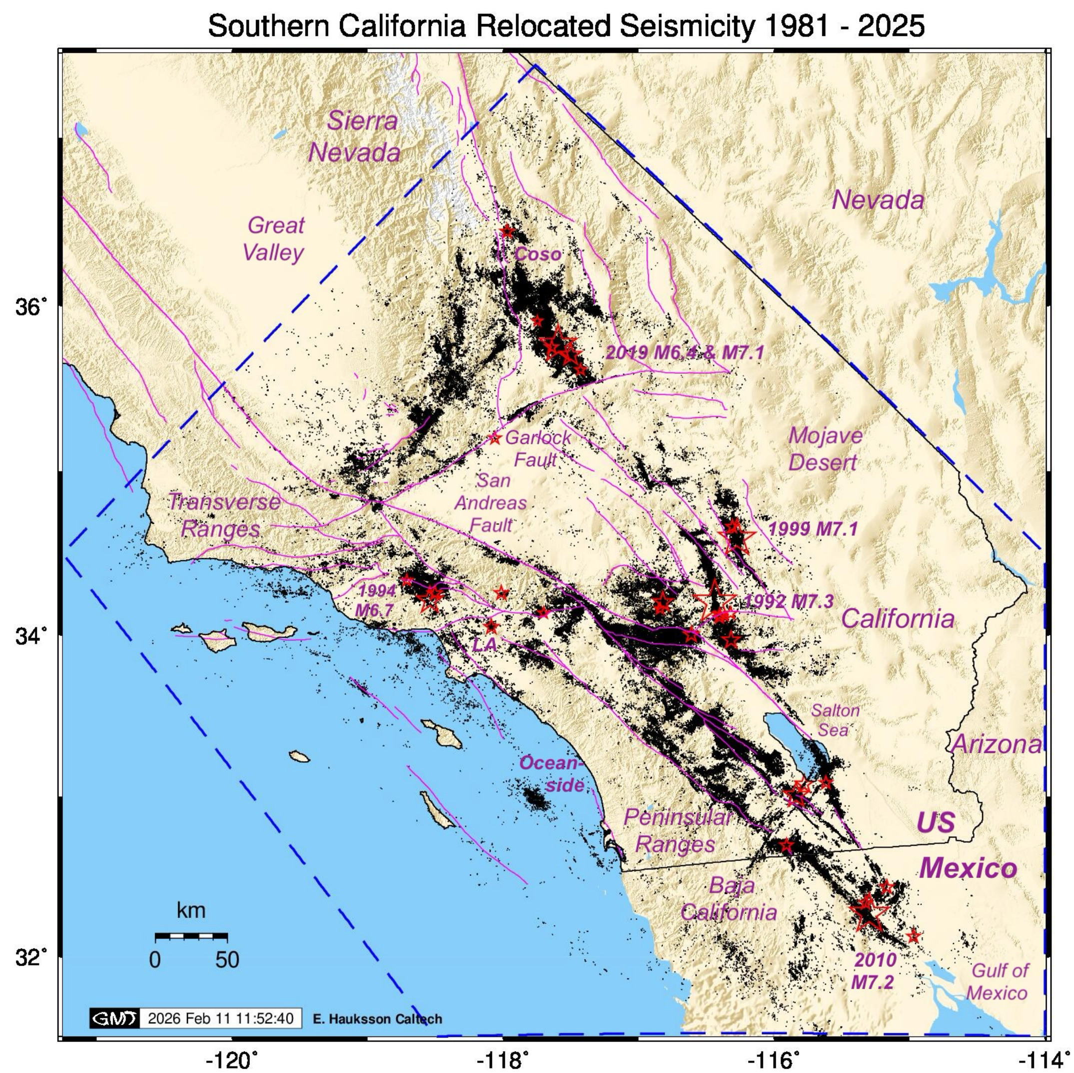

Figure 1. *The HS catalog (1981 – 2025). Similar-event clusters that have been relocated by using waveform cross-correlation and GrowClust are shown in black. Uncorrelated events are not plotted. Events with M ≥ 5.5 are shown as red stars. Faults are from Jennings and Bryant (2010) with late Quaternary faults shown in magenta color. The blue dashed polygon delineates the SCSN reporting area. LA: City of Los Angeles.*

The quality of the catalog changes over time because new stations were added or upgraded, and the processing of the data has improved. In Figure 2 (left) we show the magnitude of the different types of

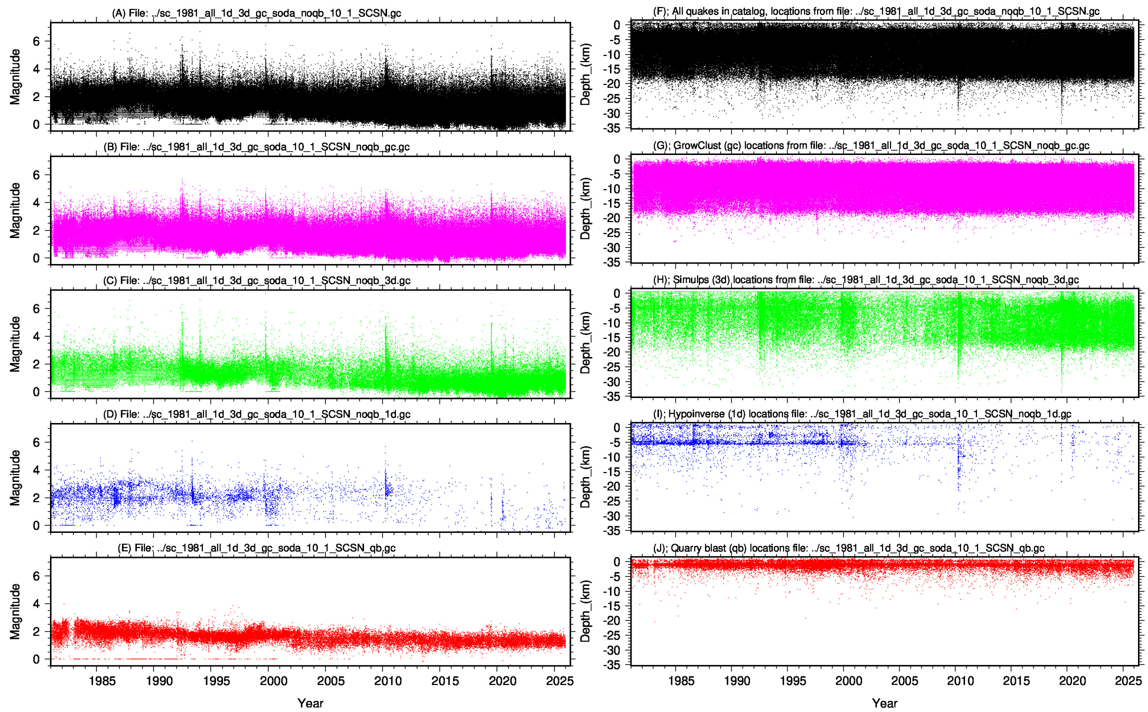

Figure 2. *Magnitude and depth for the different components of the HS catalog (1981 – 2025). The "Complete Catalog" in black includes all locations. The "GrowClust locations" in magenta, include only events that qualified for GrowClust solutions. The 3d in green and 1d in blue are events of lower quality that only qualified for a 3d (intermediate quality) or 1d (lowest quality) locations.*

events in the catalog as a function of time for 45 years. The "complete catalog" panel includes all events. The 3d and 1d events are events of lower quality that do not qualify for a GrowClust location. The ~41,000 quarry blast relocations are not included in the relocated HS catalog but are available separately. In Figure 2 (right), we show the same datasets plotted versus time and depth. The GrowClust located events are well constrained in the depth range from 0 to ~20 km. Only the 3d and 1d locations show increased deep activity immediately following large (~M7) events. In many cases the 1d Hypoinverse solutions clearly have unconstrained depths, which causes the apparent concentration of many of the hypocenters at similar depths, like at ~5 km depth. Similarly, the quarry blasts are mostly scattered in the depth range from 0 km to ~ 3 km, which depends on station coverage adjacent to each quarry.

Results: Depth Distributions of Focal Depths in the HS Catalog

The HS catalog includes all SCSN recorded events. About 87% of the events qualify for cross-correlation and GrowClust relocation; another 12% qualified for only phase picks and 3d-model SIMULPS relocation, while 1% of the events only qualified for phase picks and 1d-model Hypoinverse relocation.

Because not all earthquakes qualify for the best possible relocation with GrowClust, we need to pay attention to if the quakes located with only Simulps (3d model; *Thurber*, 1993) or Hypoinverse (1d model; *Klein*, 2002) affect the overall depth distribution.

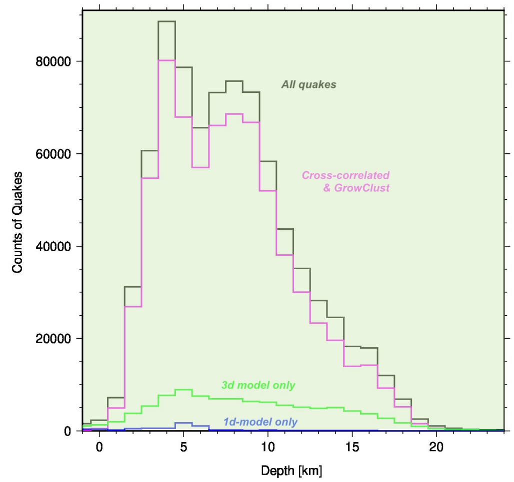

Figure 3. *Binned histograms of counts of earthquakes (1981 - 2025) versus focal depth. All the quakes in the catalog (black); GrowClust relocated (magenta); Simulps using the 3d velocity model (green; Hypoinverse using a 1d velocity model (blue).*

The binned histograms of focal depth distributions in Figure 3A demonstrate that the small number of (3d-model, Simulps and 1d-model, Hypoinverse only) events does not significantly affect the total focal depth distribution, which extends from 0 km to 20 km depth, referred to mean sea level.
Most of the moderate-sized events of M> 4.5 do not cross-correlate with smaller events and are located only with Simulps and therefore are a significant part of the 3d-model histogram. The 3d-model only cumulative histograms in Figure 3B indicates that events of M > 4.5, which are often mainshocks, can on average have deeper focal depths by up to 2 km in the depth range of 8 to 15 km. In contrast, all the only Hypoinverse relocated events are of small magnitude and located at shallow focal depth, by 3 to 5 km, than the GrowClust events. Because these are few 1d-model events (6,707), they do not significantly affect the properties of the whole catalog.

Results: Seismicity Rate: 19981 – 2025

In this study we analyzed the complete SCSN catalog, which includes earthquakes that have occurred in several different tectonic regions as well as other sources of seismicity, such as induced seismicity in geothermal fields.

The rate of M≥4.0 and M≥5.0 earthquakes recorded per year by the SCSN is shown in Figure 4. We have investigated the frequency of these larger events because they are felt and often attract public attention. The rate of M≥4.0 events varies randomly between five to 30 events per year. However, if a M>6.7 mainshock occurs, the rate can range from ~60 to ~189 M≥4 events per year, as was observed for the Landers quake in 1992. Most of these M≥4 events were aftershock of the respective mainshock of M>6.7. The number of M≥5.0 events rages from zero to five in a normal year but can increase up to 20 events following a M≥6.7 event.

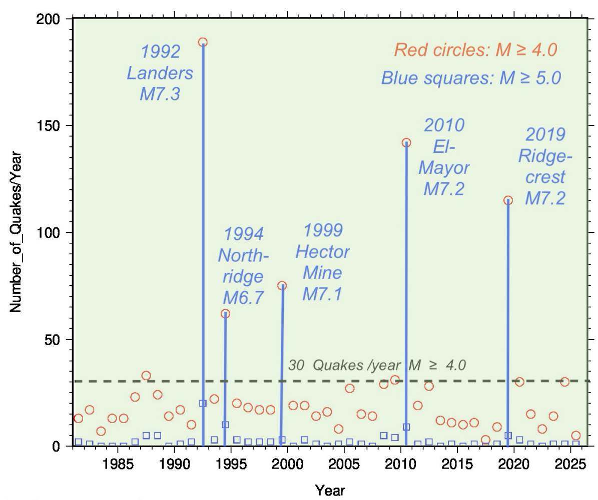

Figure 4. *Number of M ≥ 4.0 and M ≥ 5.0 earthquakes per year from 1981 to 2025. The M > 7.0 quakes are labeled and identified by blue bars.*

Although M≥6.7 mainshock seem to occur every ~10 years, temporal pattern of the occurrence of M≥4.0 events does not seem to be systematic. There is no obvious pattern of an annual increase or decrease of M4s prior to or following the M7 mainshocks. The productivity of M≥4.0 events following M7 mainshocks is highly variable depending on the tetonic regime.

Results: New Data Processing Workflow

We have worked on a new data processing workflow with the intent of using more modern software for the relocations of the whole catalog. As a 1st step would still use the Hypoinverse code for quality checks, like searching for missing stations or identifying bad stations. The 2nd step has been to implement **NonLinLoc (NLLoc)** with a one-dimensional velocity model. A future step could be to implement a 3D velocity model in the NLLoc framework but that will require some code modifications to the publicly available NLLoc code base. The third step will use **GrowClust3D.jl (GC3D)** algorithm (*Trugman et al*., 2022) but producing such a final GC3D catalog is work in progress.

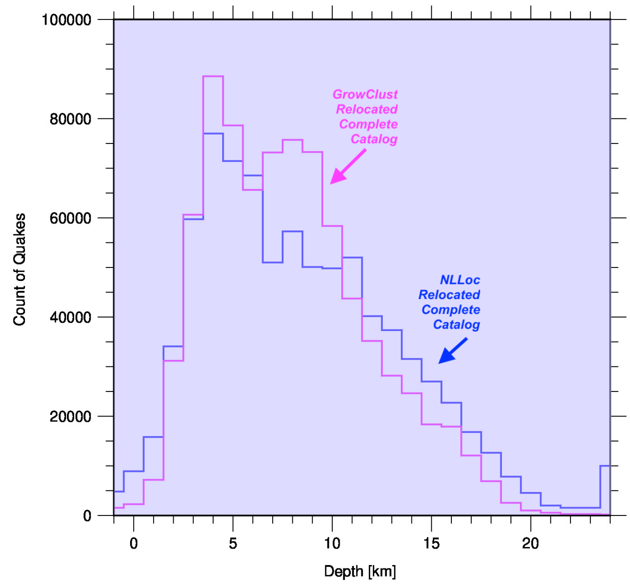

Figure 5. *Binned histograms of counts of earthquakes (1981 - 2025) versus focal depth. The GrowClust relocated (magenta);NonLinLoc using a 1d velocity model (blue).*

Absolute So Cal NonLinLoc Catalog

Originally the NonLinLog algorithm was developed by *Lomax et al*. (2000; 2022) to determine earthquake locations as a probability cloud in 3D space. Since then, the algorithm has been improved, and various bug fixes have been implemented. For determining absolute locations, we have used travel-time tables calculated from a southern California 1D velocity model. In the future, we plan to use the 3D velocity model (CVM-S4.26) from *Lee and Chen*, 2016) and/or the *Hauksson* (2000) 3D-model to calculate travel-time tables for the ~2000 stations with the NLLoc algorithm. This algorithm calculates a probability density function (PDF) in 3D space, which contains a complete description of possible hypocenter locations and thus complete uncertainty information.

The Depth distribution of the ~832,000 hypocenters determined with GrowClust and NLLoc are compared in Figure 5. There are some surprising differences, especially below ~6 km depth. The GrowClust hypocenter cluster in the depth range of 3 to 10 km but the NLLoc show a narrower peak between 3 and 6 km depth. In the range from 11 to 21 km the NNLoc hypocenters are consistently deeper by a 1.0 km.

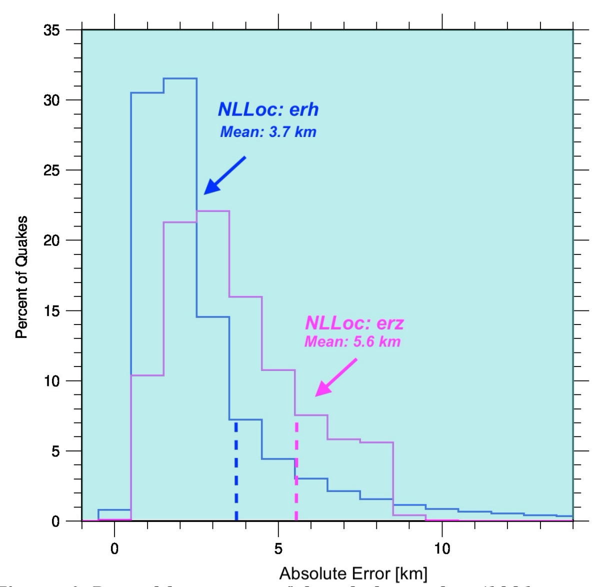

Figure 6. *Binned histogram of the whole catalog (1981 – 2025) showing the absolute horizontal and vertical location errors determined by NLLoc . The average errors are labeled with, erh=3.7 km and erz =5.6.*

The strength of NLLoc is to provide reliable hypocenter error estimates. *Hauksson et al.,* (2012) provided absolute horizontal 1-sigma error estimates of about 1 km, and depth errors of about 2 km for an earlier version of the SCSN relocated catalog. The NLLoc errors, derived from the covariance matrix of the probability density function (PDF), are about 3 times larger, which illustrates the difference in the two location methods. They are similar to 3-sigma errors determined by Hypoinverse. These errors depend on availability of both P and S picks within short epicentral distances and with a fairly even azimuthal distribution.

Results: Focal catalog of mechanisms (1981-2025)

Yang et al. (2012) determined a large, refined catalog of focal mechanisms for 1981 to 2010 using the HASH method of *Hardebeck and Shearer* (2002, 2003). Both P-wave first motion polarities and S/P amplitude ratios are used to calculate these focal mechanisms. We continue updating this 45-year-long catalog by including new events that occurred in 2025, using the latest relocated hypocenters. As an example, A and B quality focal mechanisms for 2025 are shown in Figure 7.

We have added the following recent improvements to our focal mechanism processing: 1) the capability to use the latest relocations from the refined catalog; 2) modified scripts to use already-downloaded SAC waveforms; 3) corrected the code to better include known instrument reversals by referring to station by net code, station, code and location code. The 1981-2025 focal mechanisms catalog for the SCSN reporting area can be downloaded from here:

http://scedc.caltech.edu/research-tools/alt-2011-yang-hauksson-shearer.html

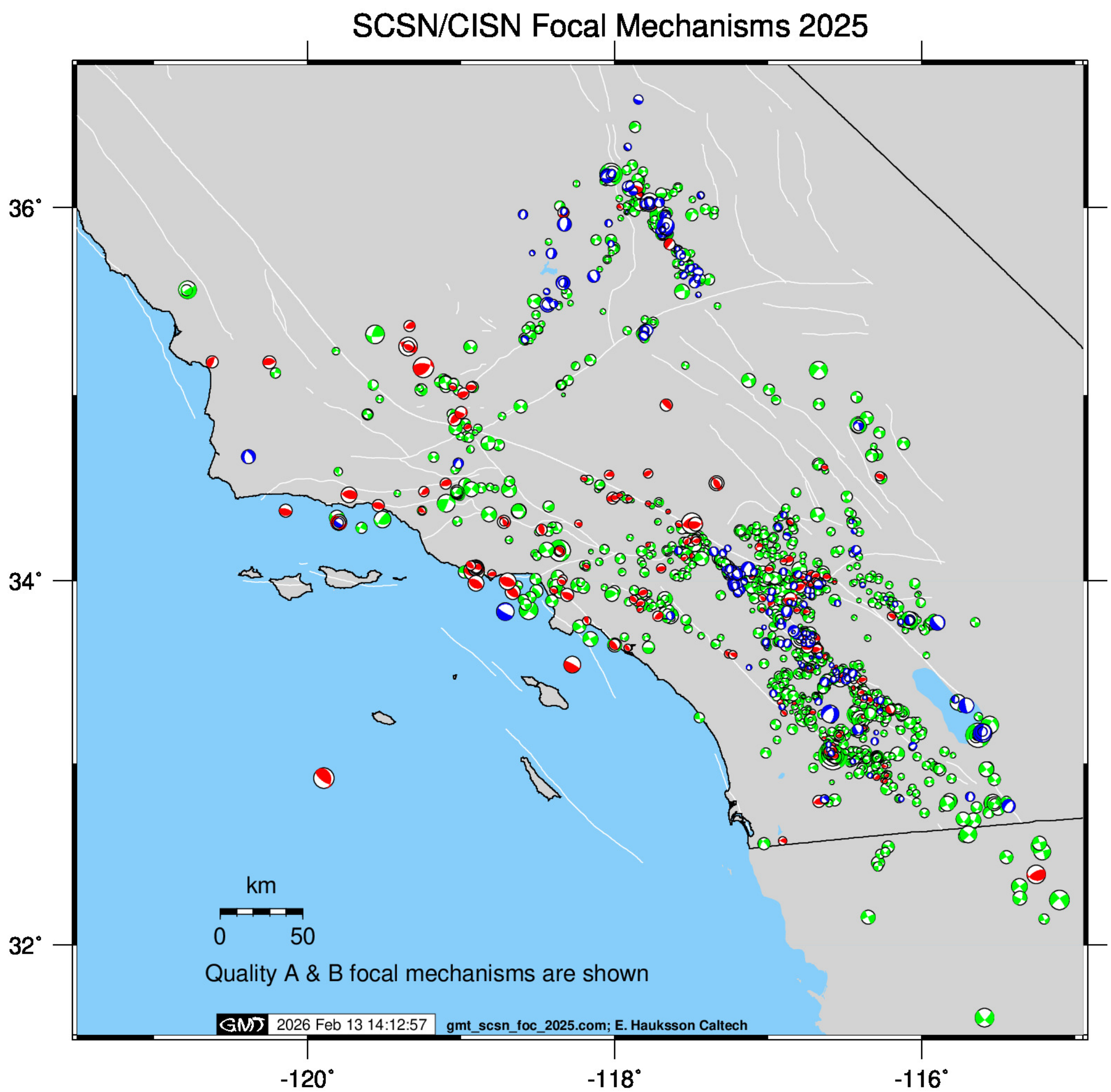

Figure 7. *A and B quality focal mechanisms of the seismicity in 2025. Strike-slip mechanisms are shown in green; thrust in red; and normal in blue. Late Quaternary faults are shown in white color (Jennings and Bryant (2010).*

Acknowledgements

This research was supported by the Southern California Earthquake Center. SCEC is funded by NSF Cooperative Agreement & USGS Cooperative Agreement. The SCSN is partially funded by USGS Cooperative Agreement, and CalOES Agreement with Caltech. We have used waveforms and parametric data from the Caltech/USGS Southern California Seismic Network (SCSN); doi: 10.7914/SN/CI; stored at the Southern California Earthquake Data Center. doi:10.7909/C3WD3xH1. We used GMT from *Wessel et al*. (2013) to make the Figures.

Project presentations and publication (in approximate publication order)

Hauksson, E., Jones, L. M., Stock, J. M., & Husker, A. L. (2024). Synthesis of current seismicity and tectonics along the 1857 Mw7.9 Fort Tejon earthquake rupture and the southernmost San Andreas Fault, California, USA. Journal of Geophysical Research: Solid Earth, 129, e2024JB028893. https://doi.org/10.1029/2024JB028893

Hauksson, E. (2024). High Resolution Catalogs of Template Earthquakes and Focal Mechanisms for Resolving Fine-Scale Fault Structures and Crustal Rheology in Southern California. Poster Presentation at 2024 SCEC Annual Meeting.

References (Publications listed above are not included).

Chen, X., and P. M. Shearer (2011), Comprehensive analysis of earthquake source spectra and swarms in the Salton Trough, California, J. Geophys. Res., 116, B09309, doi:10.1029/2011JB008263.

Hauksson, E., Crustal structure and seismicity distributions adjacent to the Pacific and north America plate boundary in southern California, *J. Geophys. Res.*, *105*, 13,875-13,903, 2000.

Hauksson, E., W. Yang, and P. Shearer, Waveform relocated earthquake catalog for southern California (1981 to June 2011), *Bull. Seismol. Soc. Am.*, 102, 2239–2244, doi: 10.1785/0120120010, 2012.

Hauksson, E. and M.-A. Meier (2018). Applying Depth Distribution of Seismicity to Determine Thermo-mechanical Properties of the Seismogenic Crust in Southern California: Comparing Lithotectonic Blocks; *Pure and Applied Geophysics*, https://doi.org/10.1007/s00024-018-1981-z

Hauksson, E. J. M. Stock, and A.L. Husker (2022) Seismicity in a weak crust: the transtensional tectonics of the Brawley Seismic Zone section of the Pacific-North America Plate Boundary in Southern California, USA. *Geophys. J. Int. (2022) 231, 717-735, https://doi.org/10.1093/gji/ggac205*

Hardebeck, J.L. and P.M. Shearer, A New Method for Determining First-Motion Focal Mechanisms, *Bull. Seismol. Soc. Am. 92,* 2264-2276, 2002.

Hardebeck, J.L. and P.M. Shearer, Using S/P amplitude ratios to constrain the focal mechanisms of small earthquakes, *Bull. Seismol. Soc. Am*., **93**, 2434-2444, 2003.

Jennings, C.W., Bryant, W.A., 2010. 2010 Fault Activity Map of California. Geologic Data Map No. 6, California Geological Survey, Sacramento CA.

Klein, F. W., User's Guide to HYPOINVERSE-2000, a Fortran Program to Solve for Earthquake Locations and Magnitudes, U.S. Geological Survey, *Open File Report 02-171*, Menlo Park, California, 2002.

Lee, E.-J. and Chen, P., (2016). Improved Basin Structures in Southern California Obtained Through Full-3D Seismic Waveform Tomography (F3DT), 87, Seismological Research Letters , DOI 10.1785/0220160013.

Lomax A., Virieux J., Volant P., Berge-Thierry C. (2000) Probabilistic Earthquake Location in 3D and Layered Models. In: Thurber C.H., Rabinowitz N. (eds) Advances in Seismic Event Location. Modern Approaches in Geophysics, vol 18. Springer, Dordrecht. https://doi.org/10.1007/978-94-015-9536-0_5

Lomax, A., and A. Savvaidis (2022). High-precision earthquake location using source-specific station terms and inter-event waveform similarity, J. Geophys. Res. 127, e2021JB023190, doi: 10.1029/2021JB023190.

Plesch, A., J. H. Shaw, Z. E. Ross, and E. Hauksson (2020). Detailed 3D Fault Representations for the 2019 Ridgecrest, California, Earthquake Sequence, Bull. Seismol. Soc. Am. 110, 1818–1831, doi: 10.1785/0120200053

Ross, Z. E., D. T. Trugman, E. Hauksson, P. M. Shearer (2019). Searching for Hidden Earthquakes in Southern California, *Science,* 10.1126/science.aaw6888 (2019).

Shearer, P. M., Abercrombie, R. E., & Trugman, D. T. (2022). Improved stress drop estimates for M 1.5 to 4 earthquakes in southern California from 1996 to 2019. Journal of Geophysical Research: Solid Earth, 127, e2022JB024243. https://doi.org/10.1029/2022JB024243

Tape, C., Q. Liu, A. Maggi, and J. Tromp (2009), Adjoint tomography of the southern California crust, Science , 325 , 988–992, doi:10.1126/science.1175298.

Thurber, C. H., Local earthquake tomography: Velocities and V_p/V_s-Theory, in *Seismic Tomography: Theory and Practice*, edited by H. M. Iyer and K. Hirahara, pp. 563-583, Chapman and Hall, London, 1993.

Trugman, D. T., and P. M. Shearer (2017). GrowClust: A Hierarchical Clustering Algorithm for Relative Earthquake Relocation, with Application to the Spanish Springs and Sheldon, Nevada, Earthquake Sequences, *Seismol. Res. Lett.* , 88 (2A), 379–391, doi:10.1785/0220160188 .

Lomax A., Virieux J., Volant P., Berge-Thierry C. (2000) Probabilistic Earthquake Location in 3D and Layered Models. In: Thurber C.H., Rabinowitz N. (eds) Advances in Seismic Event Location. Modern Approaches in Geophysics, vol 18. Springer, Dordrecht. https://doi.org/10.1007/978-94-015-9536-0_5

Lomax, A., and A. Savvaidis (2022). High-precision earthquake location using source-specific station terms and inter-event waveform similarity, J. Geophys. Res. 127, e2021JB023190, doi: 10.1029/2021JB023190.

van der Elst, N. J., and B. E. Shaw (2015), Larger aftershocks happen farther away: Nonseparability of magnitude and spatial distributions of aftershocks, Geophys. Res. Lett., 42, 5771–5778, doi:10.1002/2015GL064734.

Wessel, P., Smith, W. H. F., Scharroo, R., Luis, J. F., & Wobbe, F. (2013). Generic Mapping Tools: Improved version released. *EOS Trans AGU*, *94*, 409–410.

Yang, W., E. Hauksson, and P. Shearer, Computing a large refined catalog of focal mechanisms for southern California (1981 – 2010): Temporal Stability of the Style of Faulting; *Bull. Seismol. Soc. Am.*, 102, 1179–1194, doi: 10.1785/0120110311, 2012.

Yang, W. and E. Hauksson, The tectonic crustal stress field and style of faulting along the Pacific North America Plate boundary in Southern California, *Geophys. J. Int.* (July, 2013) 194 (1): 100-117 first published online April 22, 2013 doi:10.1093/gji/ggt113

Zaliapin, I., & Ben-Zion, Y. (2020). Earthquake declustering using the nearest-neighbor approach in spacetime-magnitude domain. Journal of Geophysical Research: Solid Earth, 125, e2018JB017120. https://doi.org/10.1029/2018JB017120